International Journal of GEOMATE, Oct. 2023, Vol. 25, Issue 110, pp.77-86
ISSN: 2186-2982 (P), 2186-2990 (O), Japan, DOI: https://doi.org/10.21660/2023.110.3957
Geotechnique, Construction Materials and Environment

FLOW CHARACTERISTICS OF EQUILIBRIUM AND NON-EQUILIBRIUM SEDIMENT TRANSPORT FLOWS

Miskar Maini[1,2], *Bambang Agus Kironoto[1], Adam Pamudji Rahardjo[1] and Istiarto[1]

[1]Department of Civil and Environmental Engineering, Faculty of Engineering, Universitas Gadjah Mada, Indonesia
[2]Department of Civil Engineering, Faculty of Infrastructure and Regional Technology, Institut Teknologi Sumatera (ITERA), Indonesia

*Corresponding Author, Received: 29 May 2023, Revised: 27 July 2023, Accepted: 3 Aug. 2023

ABSTRACT: Sediment transport in a river segment can be in equilibrium or non-equilibrium, depending on the amount of sediment entering and leaving the segment. The sediment transport flow can cause the riverbed to either remain stable or become unstable, resulting in either degradation or aggradation of the riverbed. This study evaluates the effect of equilibrium and non-equilibrium sediment transport on flow characteristics such as velocity, turbulence intensity, and Reynolds shear stress. Experiments were conducted with (SF) and without sediment feeding (NSF) to represent the laboratory's two sediment transport conditions. One hundred and twenty mean velocity and turbulence profiles were measured using an Acoustic Doppler Velocimeter in movable bed flows with sediment transport. The flow velocity profile with sediment feeding tends to become more slender than that without sediment feeding. The velocity profile in the inner region decreases and increases in the outer region. The friction velocity, u_*, and the integration constant of the logarithmic law, *Br*, which decreases closer to the channel side wall, show a more pronounced trend for the data with sediment feeding. The data on turbulence intensities of u'/u_*, v'/u_*, w'/u_*, follows an exponential law pattern; clear distinctions are observed between flows with and without sediment feeding. The measurement of Reynolds shear stress $-\overline{u_f v_f}/u_*^2$ displays a linear trend of shear-stress distribution. The suppression of Reynolds shear stress is observed and is more pronounced closer to the channel bed ($y/H < 0.15 – 0.2$) and towards the channel side wall, especially for the flow with sediment feeding.

Keywords: Sediment transport, Equilibrium and non-equilibrium, Velocity, Turbulence

1. INTRODUCTION

Sediment transport in open channels is a complex phenomenon influenced by various hydraulic and river geomorphological factors. Conversely, sediment transport also significantly affects flow characteristics in open channels, such as velocity and turbulence, which are important for river improvement and planning. Many researchers have extensively studied these flow characteristics, either for clear water flows and flow with sediment transport or by developing empirical and semi-empirical models for various purposes of research and development of water infrastructure. This approach is based on observation and experimental data on clear water flow in smooth and gravel-bed without bed loads [1,2] and movable gravel-bed with bed loads [3]. In addition to clear water flow, previous research has also studied sediment-laden flow based on laboratory experiments [4], and suspended sediment studies based on field case studies of rivers and lakes have also been examined [5,6]. However, despite the significant contributions of previous studies to understanding flow characteristics, there still needs to be a gap in fully discussing the differences in flow behavior under clear water, equilibrium, and non-equilibrium sediment transport conditions. In flow conditions with equilibrium sediment transport, the riverbed remains stable. In contrast, in non-equilibrium sediment transport conditions, the riverbed experiences aggradation and degradation, resulting in variations in flow characteristics. These variations, in turn, will influence the river's overall behavior concerning river improvement and planning.

In recent years, research on flow characteristics, such as velocity and turbulence in open channels, has made remarkable progress due to the use of high-resolution instrumentation. These advanced instruments, including the Acoustic Doppler Velocimeter (ADV) instrument [7–9] and the Particle Image Velocimeter (PIV) method [10,11], enable more accurate measurements of flow velocity and turbulence, as demonstrated in this present study and others.

In this study, the Acoustic Doppler Velocimeter (ADV), a well-tested and accurate instrument, was used to focus on measuring the velocity and turbulence of equilibrium and non-equilibrium sediment transport currents. It should be noted that research of this nature is still very limited and rarely conducted by researchers in literature.

Sediment transport in a river segment can be in equilibrium or non-equilibrium, depending on the balance of sediment entering and leaving the segment, which can impact the stability of the river bed. This study investigates the impact of equilibrium and non-equilibrium sediment transport on various flow characteristics, including velocity, turbulence intensity, and Reynolds shear stress. The research was conducted in a laboratory setting, using a movable bed flume to measure velocity and turbulence profiles with and without sediment feeding. Sediment feeding refers to flows with balanced (equilibrium) sediment transport and a stable river bed. In contrast, non-sediment feeding indicates an imbalance (non-equilibrium) in sediment transport that could cause erosion or deposition. It should be noted that this study only considers the effects of non-equilibrium sediment transport flows on riverbed erosion and does not address deposition situations.

Future research efforts on equilibrium and non-equilibrium sediment transport flow need to examine in more detail the relationship of influences, such as the roughness of the Manning coefficient, Chezy coefficient, shear velocity, and Reynolds stress, by estimating erosion, sediment deposition, and the evolution of the topography of the layers. Then, compare laboratory experimental studies and field measurements to study the deviation characteristics of these comparisons.

2. RESEARCH SIGNIFICANCE

This study examines sediment transport's effect on flow characteristics under equilibrium and non-equilibrium sediment transport conditions. Through an experimental approach, this study provides valuable insights into the characteristics of equilibrium and non-equilibrium sediment transport flows, which have rarely received attention in previous studies. The findings from this study are expected to contribute to the advancement of hydraulics, particularly in turbulence.

3. EXPERIMENTAL SETUP

The measurements were taken in a closed sediment recirculating flume with dimensions of 10 m in length, 0.6 m in width, and 0.45 m in height. The flume had glass walls and a smooth stainless-steel floor that was modified for the study. The flume can be tilted at slopes ranging from -1% to +5% around a pivot point. An associated pump pumped the recirculating water, and sediment was fed into the system at a maximum rate of 0.5 kg/s with a maximum particle size of 3 mm. The movable bed was made of coarse sand with uniform gradation (d_{50} = 0.92 mm) and was spread to a thickness of 10 cm. The flow discharge ranged between 35 l/s and 50 l/s with two different bed slopes of 0.15% and 0.3%. Several guiding and stabilizing devices were installed at the flume entrance to ensure a quasi-uniform entrance flow. For movable beds with equilibrium sediment transport flow, the amount of sediment transport varied between 0.0651 and 0.1815 kg/s, while for non-equilibrium sediment transport flow, it varied between 0.0125 and 0.0224 kg/s. The bed decreased by 0.5 cm to 2 cm per hour for non-equilibrium sediment transport flow, depending on the amount of sediment load transported by the flow. Equilibrium and non-equilibrium sediment transport flows were obtained by controlling the sediment feeding rate, which varied between 0.0066 kg/s and 0.110 kg/s.

Within fully developed turbulence flow, two measuring sections in the flume were located at x = 5.6 m (section 1) and x = 6.6 m (section 2) from the flume entrance. Measurements were conducted on half of the flume cross-section in both sections, considering the uniform and symmetrical shape of the flume. Five measurement verticals were selected for each section, with positions shown in Fig.1.

MicroADV 16-MHz was used to measure instantaneous velocity and turbulence using the Doppler shift principle [12]. The sampling value used for the laboratory experiment was 50 Hz. The time required to measure one point was 60 seconds, so 3000 data were obtained at one point. Each vertical profile consisted of 13 to 22 measurement points depending on the flow depth. The measurement interval was 0.25 cm in the region of $y/H \leq 0.2$ (the inner region) and 0.5 cm in the region of $y/H > 0.2$ (the outer region). The measurement points start at 0.05 cm from the bed to 5 cm from the water surface.

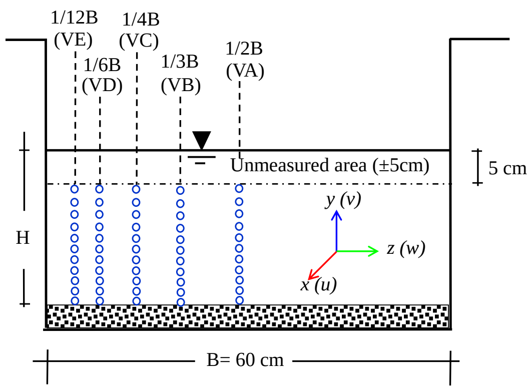

Fig.1 Arrangement of velocity measurement at a cross-section

Figure 1 shows the measurement positions for each section, showing the distance from the wall to each vertical division position. The distance in each vertical transverse direction measured from the center of the channel to the channel wall is 1/2B (VA), 1/3B (VB), 1/4B (VC), 1/6B (VD), and 1/12B (VE), where B is the width of the water level at the time of research and VA to VE are the names of the vertical division series from the center to the channel wall.

4. RESULTS AND DISCUSSION

4.1 Description of Data Acquisition

The present study measured one hundred and twenty mean velocity and turbulence profiles, comprising 12 different measurement series; all series flow with sediment transport. This series included six movable-bed without sediment feeding (NSFMBA, NSFMBB, NSFMBC, NSFMBD, NSFMBE, and NSFMBF) and six movable-bed with sediment feeding (SFMBA, SFMBB, SFMBC, SFMBD, SFMBE, and SFMBF).

The running code of the flows is based on parameters such as discharge, cross-section, and measurement location. For ease of identification, running flows are coded as follows: the code "SF" or "NSF" stands for **S**ediment **F**eeding and **N**on-**S**ediment **F**eeding flows, respectively. Furthermore, the code "MB" stands for **M**ovable-**B**ed. The codes A, B, C, D, E, and F describe discharge and channel slope variations. The next set of code numbers, 1 and 2, indicate the locations of the measurement sections, 1 and 2, which are 1 meter apart. For example, the code name for the running flow, "NSFMBA1," can be interpreted as follows: the measurement is carried out on a flow without (non) sediment feeding, where the channel bottom is movable-bed, with a particular variation of discharge/slope, and the measurement location is in section 1. The main flow parameters of the data obtained in this study are summarized in Table 1.

Table 1 Summary of main flow parameters

Run	S (-)	H (m)	B/H (-)	R (m)	T ^{o}C	Q (l/s)	U (m/s)	R_e (-)	F_r (-)	Q_s (kg/s)
NSFMBA1	0.0015	0.134	4.49	0.092	22.50	50	0.624	347867	0.55	0.0171
NSFMBA2	0.0015	0.134	4.49	0.092	26.60	50	0.624	381844	0.55	0.0171
NSFMBB1	0.0015	0.120	5.02	0.085	26.70	45	0.628	344421	0.58	0.0141
NSFMBB2	0.0015	0.120	5.02	0.085	28.80	45	0.628	360580	0.58	0.0141
NSFMBC1	0.0015	0.114	5.25	0.083	28.40	40	0.583	317757	0.55	0.0165
NSFMBC2	0.0015	0.114	5.25	0.083	28.60	40	0.583	319135	0.55	0.0165
NSFMBD1	0.0030	0.125	4.79	0.088	27.10	50	0.665	386082	0.60	0.0223
NSFMBD2	0.0030	0.125	4.79	0.088	28.50	50	0.665	398058	0.60	0.0223
NSFMBE1	0.0030	0.114	5.27	0.083	26.20	40	0.585	302774	0.55	0.0127
NSFMBE2	0.0030	0.114	5.27	0.083	29.00	40	0.585	321899	0.55	0.0127
NSFMBF1	0.0030	0.099	6.06	0.074	27.80	35	0.589	274435	0.60	0.0154
NSFMBF2	0.0030	0.099	6.06	0.074	28.20	35	0.589	276834	0.60	0.0154
SFMBA1	0.0015	0.126	4.76	0.089	22.40	50	0.661	347055	0.59	0.1487
SFMBA2	0.0015	0.126	4.76	0.089	27.30	50	0.661	387783	0.59	0.1487
SFMBB1	0.0015	0.117	5.13	0.084	22.90	45	0.641	316009	0.60	0.1194
SFMBB2	0.0015	0.117	5.13	0.084	26.40	45	0.641	342139	0.60	0.1194
SFMBC1	0.0015	0.110	5.45	0.080	21.90	40	0.606	274408	0.58	0.0974
SFMBC2	0.0015	0.110	5.45	0.080	27.80	40	0.606	313640	0.58	0.0974
SFMBD1	0.0030	0.116	5.17	0.084	21.90	50	0.718	343010	0.67	0.1814
SFMBD2	0.0030	0.116	5.17	0.084	26.30	50	0.718	379311	0.67	0.1814
SFMBE1	0.0030	0.107	5.61	0.079	22.40	40	0.623	277644	0.61	0.1041
SFMBE2	0.0030	0.107	5.61	0.079	27.50	40	0.623	311589	0.61	0.1041
SFMBF1	0.0030	0.097	6.19	0.073	22.90	35	0.601	245784	0.62	0.0654
SFMBF2	0.0030	0.097	6.19	0.073	28.80	35	0.601	280451	0.62	0.0654

Note: B: channel width (= 0.60 m); d_{50}: median diameter of particle (= 0.92 mm); S: channel slope; H: flow depth; R: hydraulic radius (=A/P); B/H: aspect ratio; U: cross-section mean velocity $(= Q/A)$; Re: Reynolds number $(= 4UH/\nu)$; Fr: Froude number $\left(= U/\sqrt{gH}\right)$, Q: flow discharge; Q_s: measured sediment bed load.

4.2 Characteristics of Velocity Distribution and Shear Velocity

Velocity measurement data for a rough boundary, measured within the inner region, limited by $y/H < 0.2$, can be presented using the universal law of the wall, as described by Kironoto and Graf [2], as:

$$\frac{u}{u_*} = \frac{1}{\kappa} ln\left(\frac{y}{k_s}\right) + Br \tag{1}$$

Where u is the mean point velocity at a distance y measured from the reference level; u_* is the shear velocity, κ is Karman constant, Br is a numerical constant of integration, and k_s, is the equivalent sand roughness of Nikuradse. Fig.2(a) and Fig.2(b) present the typical velocity profiles measured at cross-sections from the center to the edge of the channel in the transverse direction (see also Fig.1) for both flows with and without sediment-feeding. The figure shows that the flow velocity decreases closer to the channel edge due to shear with the wall. Fig.2(c) shows a comparison between flow without sediment feeding (run NSFMBA1) and flow with sediment feeding (run SFMBA1); the plotted data are only for the velocity profiles measured at the center of the channel (z/B =0.5; VA). The figure clearly shows a difference in u/U when viewed from the velocity profile shape, where the velocity profile for the flow with sediment feeding tends to become more slender than the flow without sediment feeding. In the inner region, the velocity profile for the flow with sediment feeding decreases. In contrast, in the outer region, it increases, as indicated by the direction of the arrows in the figure.

Kironoto and Graf [2] showed that Clauser's method could precisely determine the shear velocity, energy gradient, and Reynolds stress methods. Fig.3(a) displays velocity profiles measured in movable beds with sediment feeding (SFMBB2), presented in wall coordinates (u/u_* vs. y/k_s). Equation (1) confirms that the log law adequately explains the inner region data. However, it is essential to note that the log law cannot explain the data in the outer region, where the deviation is more significant, especially for the flow with sediment feeding. In Fig.3(b), shear velocities at specific positions of z/B in the transverse direction, normalized with the friction velocity obtained at the center of the channel, $u_{*z/B}/u_{*VA}$, are plotted against z/B, for running NSFMBB2 and SFMBB2; the plotted data are only for the profiles measured at the center of the channel (z/B=0.5, VA; see also Fig.1). All plotted data show that the shear velocity decreases closer to the channel side wall. This decrease is seen more clearly for data with sediment feeding.

The Br-values obtained using Clauser's method are plotted against z/B, as shown in Fig.4(a), derived from the velocity profiles of all data obtained in this study (see Table 1). The figure shows that the Br-values differ for different types of data and different positions of z/B in the transverse direction. At the center of the channel, the Br-values are 7.16 ± 0.85 for a movable bed without sediment feeding and 6.88 ± 0.99 for a movable bed with sediment feeding. These values are smaller than those obtained in clear water without a bed load of a rough flow regime (Br = 8.5 ± 15%;[13]), possibly due to the presence of bed-load sediment transport. The particle Reynolds number of the present study, $(u_* k_s)/\nu$, ranges from 38.7 to 67.6, and according to Nikuradse [14], the Br-values should range from 8.6 to 8.75.

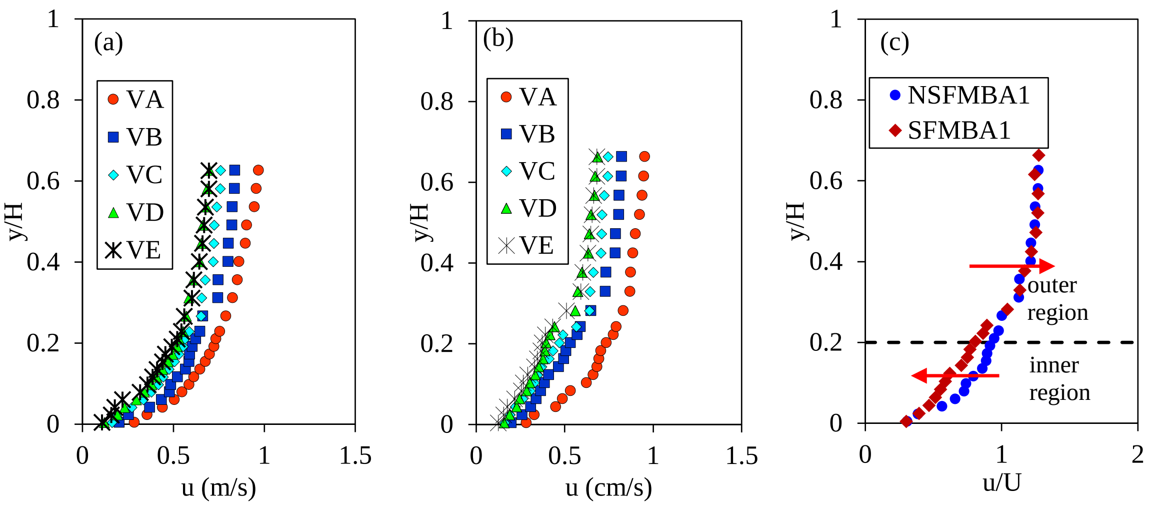

Fig.2 Typical velocity profiles, *u vs. y/H.* (a) Run NSFMBA1; (b) Run SFMBA2; (c) Comparison of velocity profiles, *u/U vs. y/H* of run NSFMBA1 and run SFMBA1 (only for the profiles at the center of the channel; z/B=0.5, VA).

The figure also shows that the *Br*-values decrease closer to the channel edge in the transverse direction (see Fig.4(a)), with a flow without sediment feeding having higher *Br*-values than sediment feeding. In general, the presence of bed-load sediment can lead to an increase in friction velocity in both running flows with and without sediment feeding. At the same time, it can cause a decrease in the Integration constant, *Br*, as shown in Fig.4(b).

4.3 Characteristics of Turbulence Intensity Distribution

The instantaneous velocities, u_i , w_i and v_i, can be written as:

$$u_i = u + u_f \tag{2}$$

$$v_i = v + v_f \tag{3}$$

$$w_i = w + w_f \tag{4}$$

Where *u*, *v*, and *w* are the mean-point velocities, u_f, v_f and w_f , is the fluctuation of the velocity components longitudinally, transversely, and vertically. The turbulence intensities, u', v', and w', are the Root Mean Square values of velocity fluctuations, calculated as:

$$u' = \sum_{i=1}^{N} \sqrt{\frac{(u_i - u)^2}{N-1}} \tag{5}$$

$$v' = \sum_{i=1}^{N} \sqrt{\frac{(v_i - v)^2}{N-1}} \tag{6}$$

$$w' = \sum_{i=1}^{N} \sqrt{\frac{(w_i - w)^2}{N-1}} \tag{7}$$

Where *N* is the number of time series values (*N* = 3000).

For uniform open channel flow, Nezu [1] suggests that the turbulence intensities are distributed according to an exponential law such as:

$$\frac{u'}{u_*} = D_1 e^{-\lambda_1\left(\frac{y}{H}\right)} \tag{8}$$

$$\frac{v'}{u_*} = D_2 e^{-\lambda_2\left(\frac{y}{H}\right)} \tag{9}$$

$$\frac{w'}{u_*} = D_3 e^{-\lambda_{13}\left(\frac{y}{H}\right)} \tag{10}$$

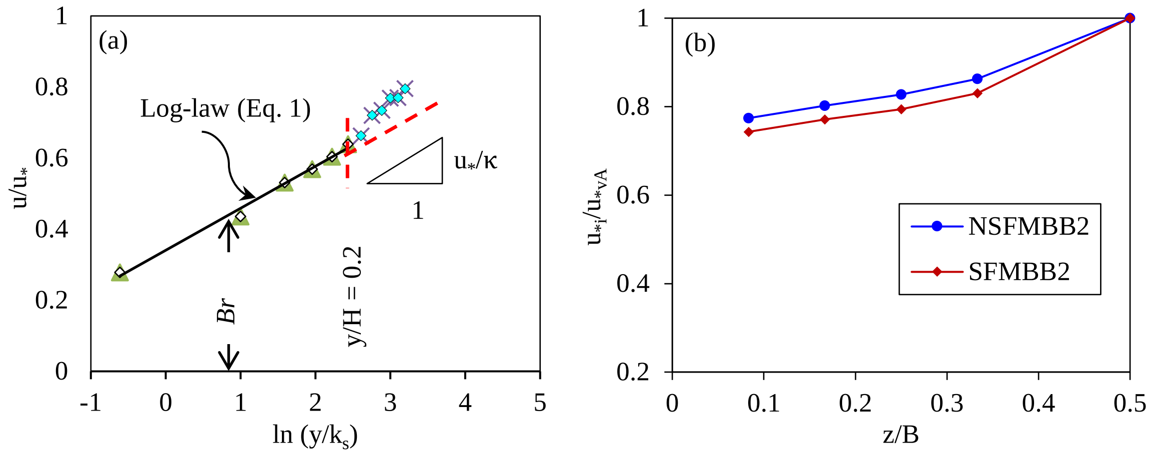

Fig.3 Clauser's method for determining shear velocity, u_*, and integration constant, *Br*. (a) u/u_* vs. ln (y/k_s) for run SFMBB2; (b) $u_{*z/B}/u_{*VA}$ vs. z/B for run NSFMBB2 and SFMBB2.

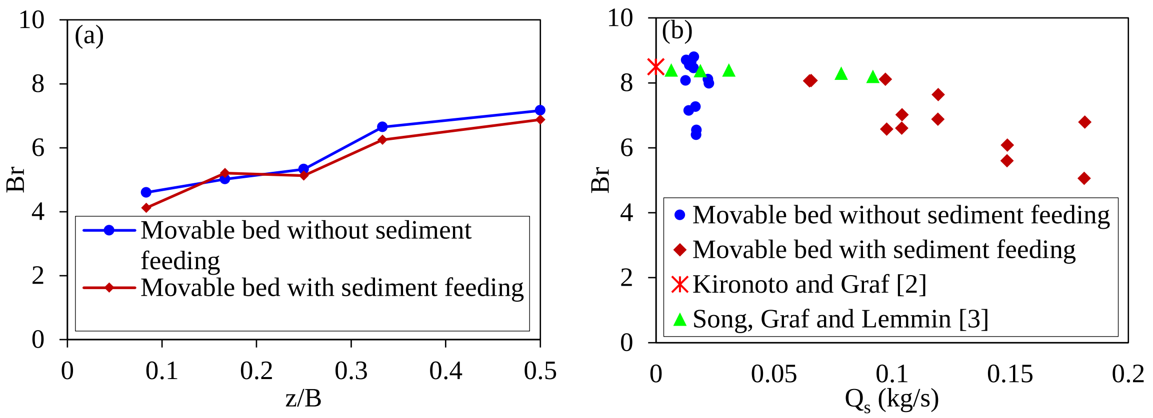

Fig.4 Integration constant, *Br*, for all of the data obtained in this study. (a) plot of *Br* vs. *z/B*; (b) plot of *Br* vs. Q_s.

where D_1, D_2, D_3, λ_1, λ_2, and λ_3 are empirical constants obtained from experimental data.

The turbulent intensity distributions of u'/u_*, v'/u_*, w'/u_* at the center of the channel (*z/B* = 0.5; VA) for two different flows, with and without sediment feeding, obtained in the present study are shown in Fig.5(a), 5(b), and 5(c), respectively. Here, u_* represents the friction velocity at the center of the channel (VA). As illustrated in the figure, the turbulence intensities of u'/u_* are greater than those of w'/u_* and v'/u_*, consistent with the findings of Nezu [1].

The data obtained in this study follows an exponential law pattern and exhibits similar trends to turbulence intensity data obtained by Kironoto and Graf [2] and by Song, Graf, and Lemmin [3] for rough/gravel bed flow without and with bed load. The data from Kironoto and Graf [2] and Song, Graf, and Lemmin [3] fall within the range of the present data. However, the trend slightly differs from the turbulence intensity data obtained by Nezu [1] for smooth bed flows. Clear distinctions were observed between flows with and without sediment feeding, with turbulence intensities in flows with sediment feeding smaller than those without sediment feeding. The feeding of sediment appears to suppress the turbulence intensity. It is important to note that the two datasets analyzed in this study are flows with bed-load transport.

The turbulent intensity values of u'/u_*, v'/u_*, w'/u_* exhibited a decreasing trend from the center of the channel (VA; *z/B* = 1/2*B*) towards the channel side wall (VE; *z/B* = 1/12*B*), as illustrated in Fig. 6 for flows without sediment feeding, and in Fig. 7 for flows with sediment feeding. This behavior may be attributed to the friction at the channel side wall, where u_* denoted as as u_{*VA}, represents the friction velocity at the center of the channel (VA). The suppression of turbulence intensities was more prominent closer to the channel bed (*y/H* < 0.15 - 0.2) and towards the channel side wall.

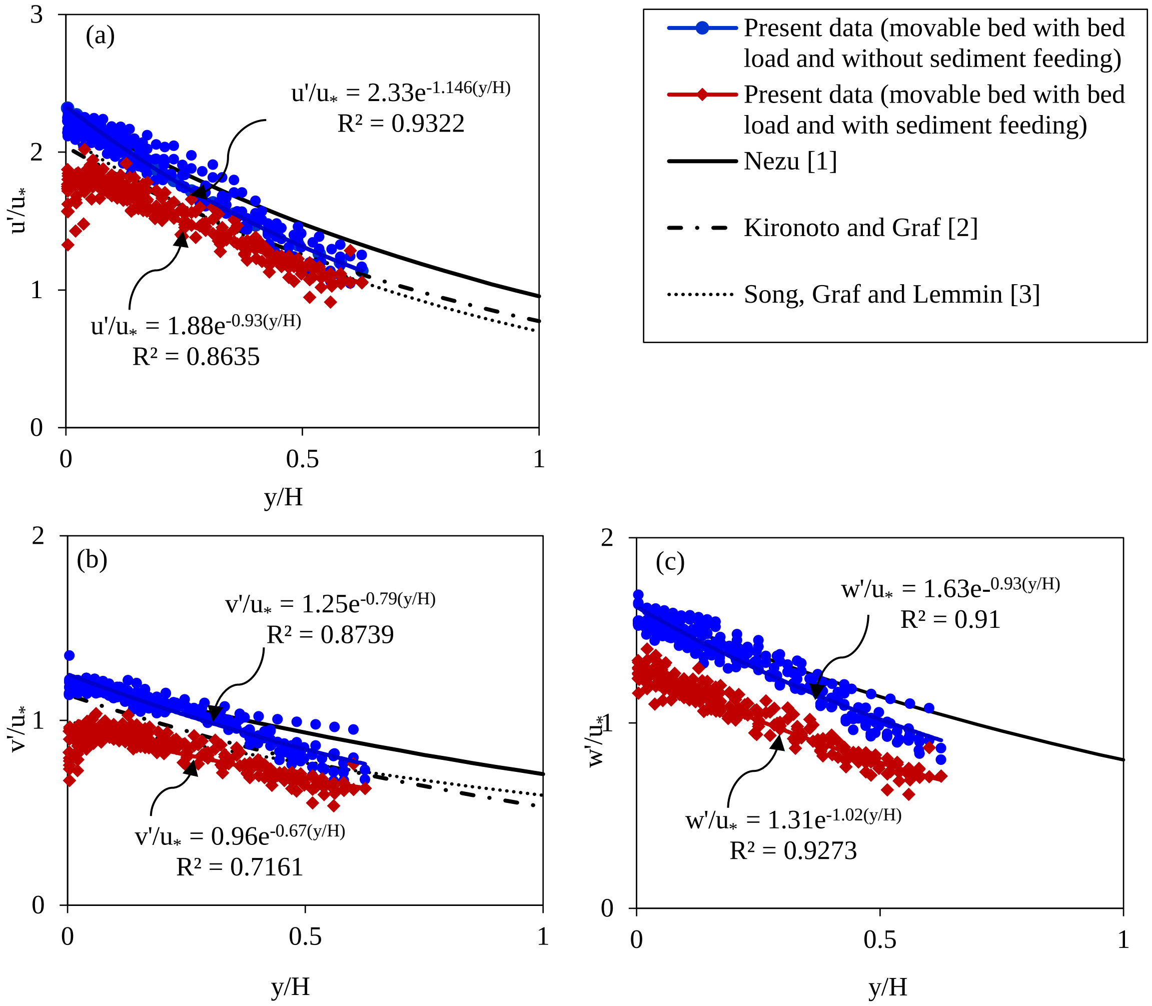

Fig.5 Turbulence intensities distribution at the center of the channel (*z/B* = 1/2*B*; VA) (a) u'/u_* vs. *y/H*; (b) v'/u_* vs. *y/H*; (c) w'/u_* vs. *y/H*

To obtain the empirical constants of Eq. (8), (9), and (10), the measured turbulence intensities, u'/u_*, v'/u_*, and w'/u_*, are fitted to the exponential law patterns proposed by Nezu [1], Eq. (8), (9), and (10). The best fit of the measured turbulence intensities data with the exponential regression equations gives the constant values of D_1, D_2, D_3, λ_1, λ_2, and λ_3. By introducing these constant values Eq. (8), (9), and (10), it can be obtained the exponential law equation for turbulence intensities. This equation is given as Eq. (11), (12), and (13) for flows without sediment feeding and as Eq. (14), (15), and (16) for flows with sediment feeding.

For flow without sediment feeding:

$$\frac{u'}{u_*} = 2.33e^{-1.15\left(\frac{y}{H}\right)} \tag{11}$$

$$\frac{v'}{u_*} = 1.25e^{-0.79\left(\frac{y}{H}\right)} \tag{12}$$

$$\frac{w'}{u_*} = 1.63e^{-0.93\left(\frac{y}{H}\right)} \tag{13}$$

For flow with sediment feeding:

$$\frac{u'}{u_*} = 1.87e^{-0.93\left(\frac{y}{H}\right)} \tag{14}$$

$$\frac{v'}{u_*} = 0.96\, e^{-0.67\left(\frac{y}{H}\right)} \tag{15}$$

$$\frac{w'}{u_*} = 1.31e^{-1.02\left(\frac{y}{H}\right)} \tag{16}$$

4.4 Characteristics of Reynolds-Stress Profile

The Reynolds shear stress distribution for uniform flow generally follows a linear distribution. The Reynolds stress is obtained by averaging their instantaneous values of $u_f v_f$ as follows:

$$-\rho\overline{u_f v_f} = \frac{1}{N}\sum_{i=1}^{N} -\rho u_f v_f \tag{17}$$

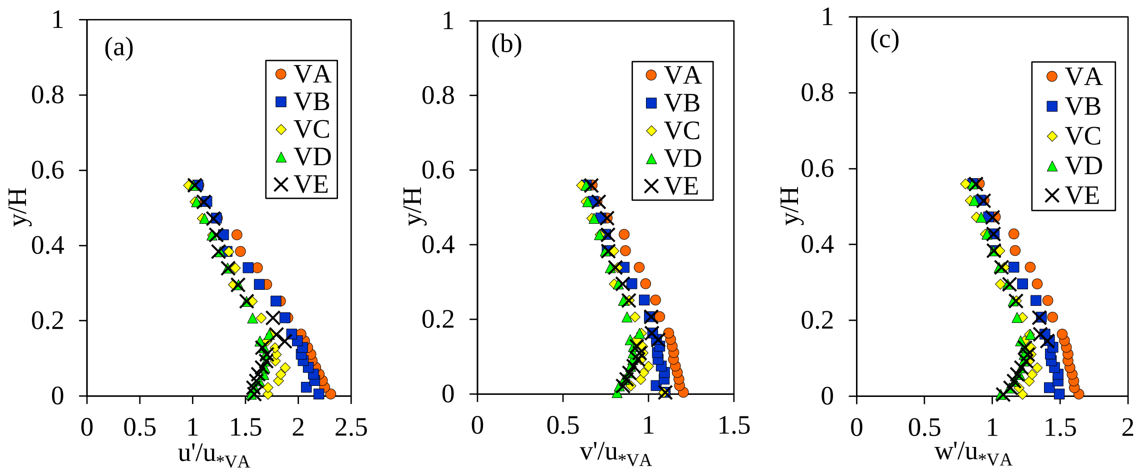

Fig.6 Turbulence intensities distribution at different measuring verticals for run NSFMBC2 (a) u'/u_{*VA} vs. *y/H*; (b) v'/u_{*VA} vs. *y/H*; (c) w'/u_{*VA} vs. *y/H*

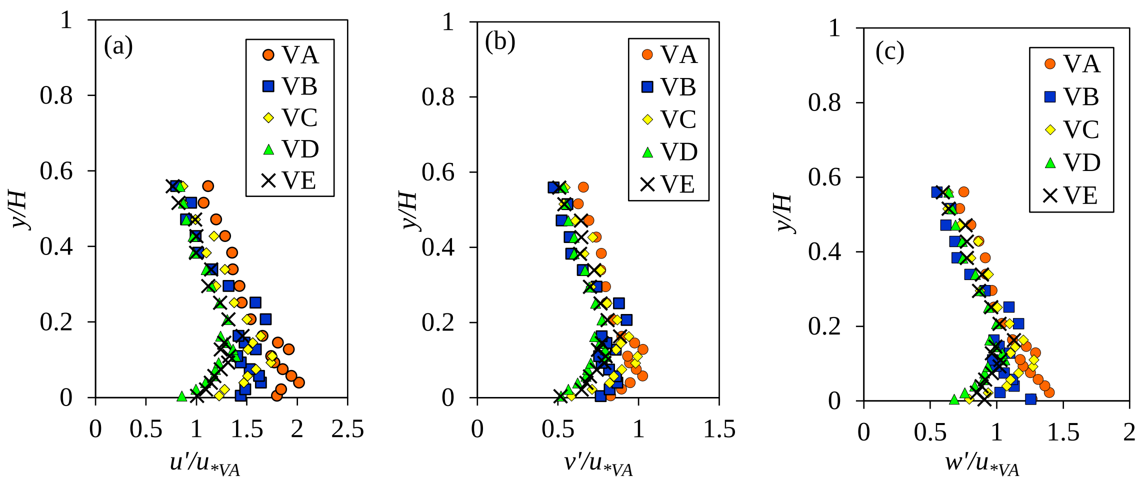

Fig.7 Turbulence intensities distribution at different measuring verticals for run SFMBC2 (a) u'/u_{*VA} vs. *y/H*; (b) v'/u_{*VA} vs. *y/H*; (c) w'/u_{*VA} vs. *y/H*.

The measured profiles of Reynolds stress $-\overline{u_f v_f}/u_*^2$, at cross sections, namely, at measuring verticals VA, VB, VC, VD, and VE (see Fig.1), are presented in Fig.8 for both flows with and without sediment feeding. In Fig.8(a) and 8(b), the shear velocity at each measuring vertical is used as the denominator, while in Fig.8(c) and 7(d), the shear velocity at the center of the channel (VA) is used as the denominator. It can be seen that the Reynolds shear stress values of flow with sediment feeding (Fig.8(d); SFMBA1) are smaller than those of flow without sediment feeding (Fig.8(c); NSFMBA1), indicating that sediment feeding suppresses the Reynolds shear stress. Although some scattered data points are observed, a linear trend of shear stress distribution can be observed. Similar to the turbulence intensity, the Reynolds shear stress values decrease from the center of the channel (VA; 1/2*B*) towards the channel side wall (VE; 1/12*B*) due to friction at the channel side wall. The results of the Reynolds-stress characteristics $-\overline{u_f v_f}\,/\,u_*^2$ show a linear trend of the distribution of Reynolds stress for flows with and without sediment feeding; its value decreases from the channel's center toward the channel's side walls.

The suppression of the Reynolds stress is observed and is more pronounced closer to the bottom of the channel (y/H < 0.15 – 0.2) and towards the side walls of the channel, especially for flows with sediment feeding (equilibrium sediment transport) which is characteristic of Reynolds-stress tends to decrease in the inner region compared to flow without sediment feeding.

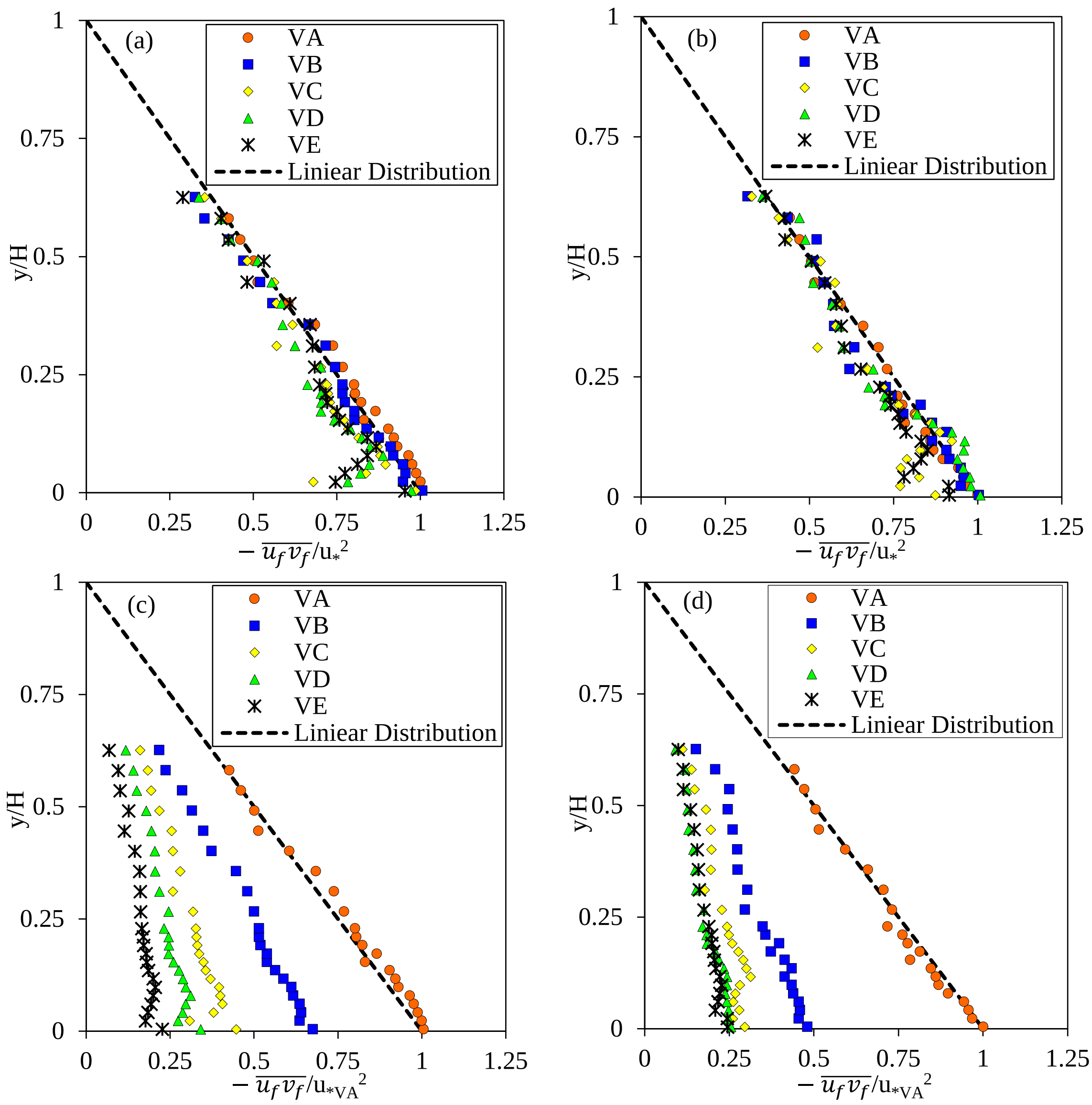

Fig.8 Reynolds-stress profiles, $-\overline{u_f v_f}/u_*^2$ vs. *y/H*.(a); (c). Flow without sediment feeding (NSFMBA1); (b); (d). Flow with sediment feeding (SFMBA1).

5. CONCLUSION

Based on the conducted studies, it can be conclusively determined that the characteristics of equilibrium and non-equilibrium sediment transport flows differ from those without sediment transport (clear water flow). Therefore, the findings of this study hold significant importance for practical applications in the field. They can aid in evaluating and estimating parameters such as flow velocity, shear velocity, Reynolds shear stress, and turbulence intensity in rivers or channels for various engineering purposes, including water infrastructure planning, navigation design, irrigation channel management, flood control, and other civil engineering applications, especially when the sediment transport plays an important role.

The specific conclusions derived from the analyzed data in this study are presented in three themes related to velocity profile, turbulent intensity, and Reynolds shear stress, as follows:

1. In the inner region, the velocity profile for flows with sediment feeding decreases, while in the outer region, it increases. The velocity profile shape, *u/U*, for the flow with sediment feeding tends to become more slender than the flow without sediment feeding. The Log-Law in Eq. (1) can predict the shear velocity, u_*, and the integration constant, *Br*, quite well. They tend to decrease closer to the side wall of the channel. This trend is more pronounced in the data with sediment feeding (flow with equilibrium sediment transport), where the shear velocity and the integration constant tend to be smaller than the flow without sediment feeding (flow with non-equilibrium sediment transport).

2. The profiles of the measured Reynolds shear stress $-\overline{u_f v_f}/u_*^2$, exhibit a similar linear trend for flows with and without sediment feeding. The value of Reynolds shear stress decreases from the channel's center towards the channel's side walls. The suppression of Reynolds stress is observed and becomes more pronounced closer to the bottom of the channel ($y/H < 0.15 - 0.2$) and towards the side walls of the channel. This effect is particularly evident in flows with sediment feeding, where the Reynolds stress tends to decrease in the inner region compared to flows without sediment feeding (non-equilibrium sediment transport).

6. ACKNOWLEDGMENTS

The authors wish to extend their sincere gratitude to the Hydraulic Laboratory at the Research Center of Engineering Science, Universitas Gadjah Mada, Yogyakarta, Indonesia, for their invaluable support during the experimental measurement process. Furthermore, the authors would like to express their deep appreciation to Institut Teknologi Sumatera (ITERA), Indonesia, for providing financial support for this research.

7. REFERENCES

[1] Nezu I., Turbulent Structure In Open Channel Flows. Doctoral Dissertation, Departement of Civil Engineering., Kyoto University, Japan (in English), 1977, pp. 1-156.

[2] Kironoto B.A., and Graf W.H., Turbulence Characteristics in Rough Uniform Open-Channel Flow. Proceeding of the Institution of Civil Engineers – Water, Maritime, and Energy. Vol.106, Issue 4, 1994, pp.333–344.

[3] Song T., Graf W. H., and Lemmin U., Uniform Flow In Open Channels With Movable Gravel Bed. Journal of Hydraulic Research, Vol. 32, Issue 6, 1994, pp. 861-876.

[4] Cellino M., and Graf W.H., Sediment-Laden Flow in Open-Channels Under Noncapacity and Capacity Conditions. Journal of Hydraulic Engineering. Vol.25, Issue 1, 1999, pp.455-462.

[5] Suif Z., Yoshimura C., Saavedra O., Ahmad N and Hul S., Suspended Sediment Dynamics Changes In Mekong River Basin: Possible Impacts of Dams and Climate Change. International Journal of GEOMATE (Geotechnique, Construction Materials, and Environment). Vol.12, Issue 34, 2017, pp.140-145.

[6] Wurjanto A., and Ajiwibowo H., Modeling The Spatial Concentration Distribution of Environmental Parameters and Total Suspended Sediment in Diatas Lake, Western Sumatra, Indonesia. International Journal of GEOMATE (Geotechnique, Construction Materials, and Environment). Vol.17, Issue 63, 2019, pp.288-296.

[7] Caroppi G., Vastila K., Gualtieri P., Jarvela J., Giugni M., and Rowinski P M., Acoustic Doppler velocimetry (ADV) data on flow-vegetation interaction with natural-like and rigid model plants in hydraulic flumes. Data in Brief, Vol. 32, Issue 5, 2020, pp. 1-9.

[8] Khuntia J.R., Devi K., and Khatua K.K., Turbulence characteristics in a rough open channel under unsteady flow conditions. ISH Journal of Hydraulic Engineering, Vol. 27, Issue 1, 2021, pp. 354-365.

[9] Rastello M., Klema M.R., Carpenter A.B., Garanaik A., Venayagamoorthy S.K, Gates T.K., and Marie J.L., Velocity measurements in developing narrow open-channel flows with high free-stream turbulence: Acoustic Doppler Velocimetry (ADV) vs Laser Doppler

Anemometry (LDA). Flow Measurement and Instrumentation, Vol.87, Issue5, 2022, pp. 1-30

[10] Das S., Balachandar R., and Barron R.M., Effect of free surface perturbation on fully developed smooth open channel flow. Journal of Hydraulic Research, Vol. 60, Issue 3, 2022, pp. 363-375.

[11] Coscarella F., Penna N., Servidio S., and Gaudio R., An experimental study on the anisotropic and intermittent behaviour of a turbulent flow over a rough bed. Journal of Physics: Conference Series, Vol. 2293, 2022, pp. 1-7.

[12] SonTek, Acoustic Doppler Velocimeter (ADV) Principles of Operation Acoustic Doppler Velocimeter (Field) Technical Documentation. San Diego, 2001.pp.1-65.

[13] Reynolds J.A., Turbulent Flows in Engineering. John Wiley and Sons Ltd., London, 1974, pp.1-462.

[14] Schlichting H., and Gersten K., Boundary Layer Theory, Springer Berlin, Heidelberg, 2016, pp.1-497.